DOI: 10.13009/EUCASS2017-169

Autoport System: a Suite of Sensors and Mechanisms for Mars UAVs

Mr. Alberto Compagnin⋆*, Mr. Enrico Lungavia*⋆*, Dr. Lorenzo Olivieri*⋆⋆
Dr. Francesco Sansone†*, Dr. Riccardo Mantellato*††*, Prof. Alessandro Francesconi*††

⋆*University of Padua*
Via 8 Febbraio 1848, 2, 35122, Padua ITALY
alberto.compagnin@studenti.unipd.it · enrico.lungavia@studenti.unipd.it
⋆⋆ *Center of Studies and Activities for Space, University of Padua*
Via Venezia, 15, 35131, Padua ITALY
lorenzo.olivieri@unipd.it
† *Stellar Project S.r.l.*
Viale Ancona, 2, 30172, Venice ITALY
francesco.sansone@stellarproject.space
††*Department of Industrial Engineering, University of Padua*
Via Venezia, 1, 35131, Padua ITALY
riccardo.mantellato@unipd.it · alessandro.francesconi@unipd.it

Abstract

In the last decades, Mars exploration has been carried out using orbiters, landers and rovers. In the future, these vehicles could be integrated with Unmanned Aerial Vehicles (UAV). Autoport is a student project of the University of Padua whose goal is to design, build and test a suite of sensors and mechanisms for autonomous Mars UAVs using COTS hardware. The features investigated are a battery recharge system, a docking mechanism and a navigation system. This paper describes the systems integrated by the Autoport Project and presents the preliminary test results conducted to validate the proposed architecture.

1. Introduction

In the last decades, the interest on planetary exploration has grown together with the constant improvements in space technology. Many probes, orbiters, landers and rovers have studied the solar system, and many more are to come in the next future. The natural development of the new technologies will end up in the employment of Unmanned Aerial Vehicles (UAVs) in planetary environments, for which many studies of feasibility have been carried out in the past years.[5,21–23] Such vehicles can provide an aerial aid to rovers and map the surrounding environment in order to improve the planning of the ground trajectory. They could be used also as explorers for the lowest layers of the atmosphere or to reach impervious sites inaccessible to rovers. These possibilities make the UAVs very attractive for future explorations.

The main crucial fields to investigate when designing a planetary UAV are the mechanics, aerodynamics and powering of the vehicle, which are still issues at the time of writing. In particular, the problem of supplying the power to the aircraft has been faced proposing the on-board production of the energy (i.e. using a small photovoltaic panel on the top of the UAV)[5] . An alternative solution is the usage of batteries which can be recharged on the mother-rover after each flight. With this method, the UAV needs to land on a recharging station and eventually dock firmly on it to recover safely during inclement weather conditions that could flip and destroy it. In this scenario, the UAV should carry on-board an integrated suite of sensors and mechanisms capable of landing the vehicle on the docking station, joining firmly to it and recharging the batteries before the next flight. As previously studied (Compagnin *et al.*[3]), such a platform needs to incorporate by three main subsystems: a navigation system dedicated to the final approach to the docking station, a docking mechanism and a battery recharge system. Each subsystem should be integrated with each other in order to occupy as less volume as possible and redundancy must be provided to prevent failures.

Many solutions have been proposed to recharge autonomously the batteries both for ground robots and terrestrial UAVs, and such technologies can be the starting point for a planetary application. Swieringa *et al.*[17] designed a mechanism

DOI: 10.13009/EUCASS2017-169

capable of swapping the battery of a small-scale helicopter without human interaction. Silverman *et al.*[16] built a passive docking station which incorporates electrical contacts to transfer energy autonomously to a small robot. A more flexible solution was proposed by Mulgaonkar[11] with a wide charging pad on which a multi-copter could land without rigid position requirements and recharge its battery using elastic contacts. A similar concept is the one of Kemper,[7] used for small helicopters and capable of operating with any orientation. In order to relax the landing requirements, the usage of Wireless Power Transfer (WPT) technology to exchange energy has been tested by Junaid[6] with a single-coil architecture and promising results. The WPT is widely used for smartphone applications thanks to its low interference with the surrounding environment and its application on UAVs has been demonstrated to be feasible by Junaid.
As said above, it is recommended for a Mars UAV to be able to joint firmly with a fixed ground station to prevent damages during inclement weather, so a docking mechanism should be provided on-board. The heritage of autonomous docking systems for small spacecrafts is wide. Pavlich[13] built and tested a mechanism specifically designed for tolerance of misalignment and scalability. The SPHERES experiment[10] uses an androgynous architecture to dock and exchange power and data and it has been successfully tested on-board the International Space Station. A semi-androgynous configuration has been designed and tested also by Olivieri[12] for small satellites application. A simpler solution has been proposed by the ARCADE experiment,[1] which uses a probe-drogue design to dock a small vehicle to a mother unit and can be the starting point in the design of a mechanism for planetary UAVs.
In order to land on the docking station, the vehicle needs a navigation system capable of determining the position and attitude during the final approach. The absence of the GNSS on a planetary environment leads the path to the state of the art on indoor navigation. Grzonka[4] managed to map an indoor environment using a laser scanner and Simultaneous Localization And Mapping (SLAM) and flew an autonomous drone inside it. Alternatively, Tournier[18] tested an algorithm for estimation and control of a UAV using a monocular camera and moiré patterns. A similar hardware has been used by Sansone,[14] involving visible LEDs and IR LEDs as targets and a camera coupled with a IR detector as sensors. Moreover, IR LEDs are the landmarks also of the solution of Wenzel,[19] who mounted a IR sensor on a UAV to determine its position and attitude with respect to a moving target which featured a IR LED pattern.
The analysis of the state of the art led to the conclusion that each of the three subsystems listed at the beginning of this introduction have been studied in depth, but there is not a global architecture for UAVs that integrates them all. In this context, Autoport is a student project of the Department of Industrial Engineering of the University of Padua whose objective is to design, build and test a docking station for Mars drones. Each subsystem must meet some requirements and constraints:

- The **Battery Recharge System** must recharge a Lithium-Polymer battery in one hour or less, balance its cells and provide redundancy;
- The **Docking Mechanism** must lock all six degrees of freedom of the UAV and resist external forces (e.g the wind). Moreover, the components mounted on the UAV must not weight more than 150 g or be larger than 100 mm x 100 mm x 100 mm;
- The **Navigation System** must determine all the six degrees of freedom of the UAV with respect to the docking station using a self-consistent system and without the aid of GNSS.

The aim is to use low-cost COTS wherever possible, to test each subsystem separately and then to integrate the components on a Flying Segment (FS) and a Ground Segment (GS), which are represented in Fig. (1). The FS is mounted on a quadrotor built with COTS from Tarot, DJI, 3DR and Futaba, while the GS is integrated in a fixed aluminum structure.

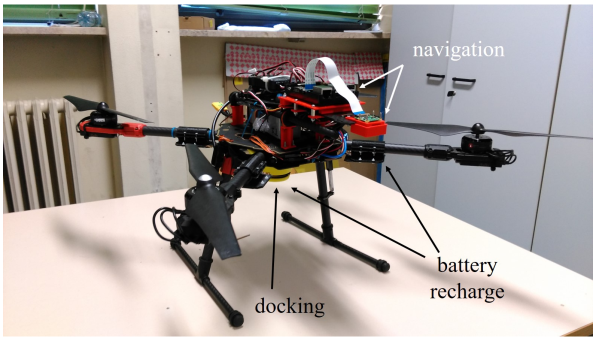

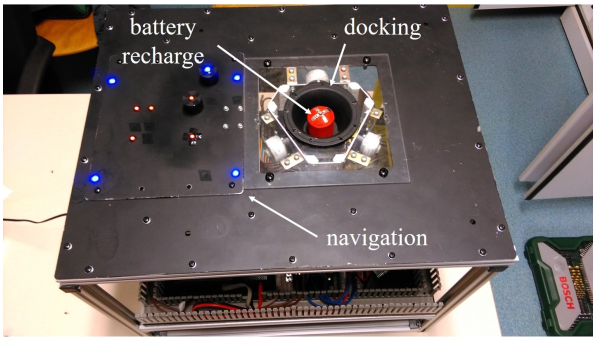

Figure 1: The Flying Segment and the Ground Segment

DOI: 10.13009/EUCASS2017-169

In the next sections, the three subsystems are presented in detail together with the preliminary tests conducted to assess their performances.

2. Overview of the subsystems

2.1 Battery recharge system

The issue of recharging autonomously the battery of a UAV is a matter of study of many research groups, as explained in the introduction. A commercial charging platform for earth drones has been developed by SkySense, but this solution is very expensive and not suitable for a docking system, such that pursued by Autoport, without heavy modifications. A solution with COTS hardware for drones capable of hard docking on a platform is still missing.
The main requirements that the Autoport Recharge System must meet are:

- to recharge a S, 5200 mAh LiPo battery at 16.8 V in one hour or less;
- to balance the four cells of the battery in order to preserve their energy storage capability and efficiency;
- to provide redundancy.

To meet these requirements, we decided to develop a hybrid system composed by a contact and a wireless interface, taking advantage of the high efficiency of a power connector and investigating the feasibility of balancing the cells of the battery using four wireless power transfer devices.
The power connector is hosted inside the docking mechanism, as displayed on the left hand side of Fig. (2) and its

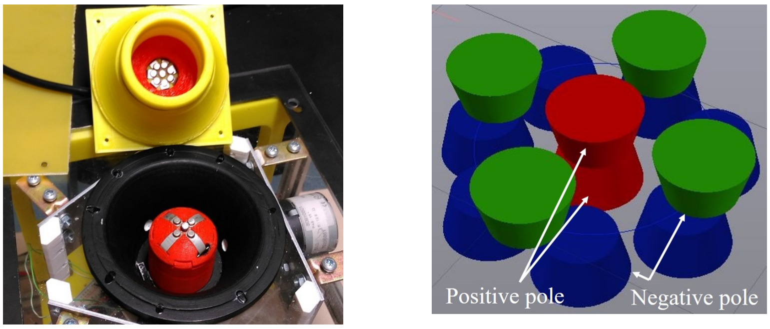

Figure 2: The power connector

poles are composed by circular rivets. The negative pole presents seven rivets on the UAV and four on the docking station, while the positive pole is composed by one rivet both on the FS and on the GS. The negative pole is circular and mounted around the positive one as represented on the right hand side of Fig. (2). This particular configuration ensured an approximate constant contact area at any yaw landing angle, both for the positive and the negative pole, resulting on a constant contact resistance in the circuit. The power connector is used to transfer most of the energy necessary to recharge the battery without balancing the cells.
The wireless interface is made up of four COTS wireless receivers and transmitters based on the Qi standard. The receivers are mounted under the arms of the quadrotor as showed in Fig. (1), while the transmitters are placed on the docking station. The components selected have an efficiency of 60% and can induce a current of 1 A at 5 V. The task of the wireless system is to balance the cells at the end of the main recharging phase, but it can be used to recharge the entire battery in the case of failure of the power connector.

2.2 Docking mechanism

The main requirements that the Autoport Docking Mechanism System must meet are:

- to facilitate the entrance of the probe into the drugue;
- to block the six degrees of freedom;
- to resist external forces;
- to be small and light-weight.

DOI: 10.13009/EUCASS2017-169

The docking mechanism is composed by a probe mounted on the lower part of the drone and a drogue fixed on the ground segment. Both part are designed in carbon fiber and the probe fits a volume of 100 mm × 100 mm × 80 mm. The first prototype has been manufactured using 3D technology on polylactic acid (PLA). The probe does not incorporate active elements, and this results in a payload weight on the drone of only 150 g.
A support structure platform for the drogue and for four locking actuators is allocated on the docking station. It is composed by six aluminum plates of 2 mm thickness that form an irregular hexagonal prism to ensure great stability and resist the load induced by the actuators or by external forces while the UAV is docked. The mechanism hosts the

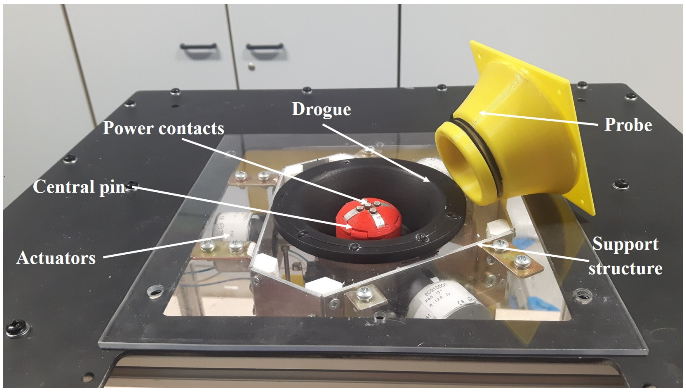

Figure 3: First Prototype Docking Mechanism

contacts of the Battery Recharge subsystem as explained in section 2.1, but is also adaptable to the use of contactless proximity power and data transfer technology (e.g. Near Field Communication) thanks to the small distance of just 6 mm between the surfaces of the probe and the drogue once the docking is accomplished. The mechanism has a very simple design and its great scalability makes it suitable for other space applications, such as cubesats, and for a wide variety of UAVs. The mechanism is axial-symmetric, therefore it does not require a particular yaw landing angle to dock properly.
The docking sequence of the mechanism consists in four steps and is represented in Fig. (4):

1. The probe enters the drogue;
2. The probe activates a contact sensor placed on the bottom of the drogue;
3. Three radial actuators are triggered and move to block the probe;
4. The central pin is moved upwards to connect the power interface with good contact pressure. Docking is accomplished.

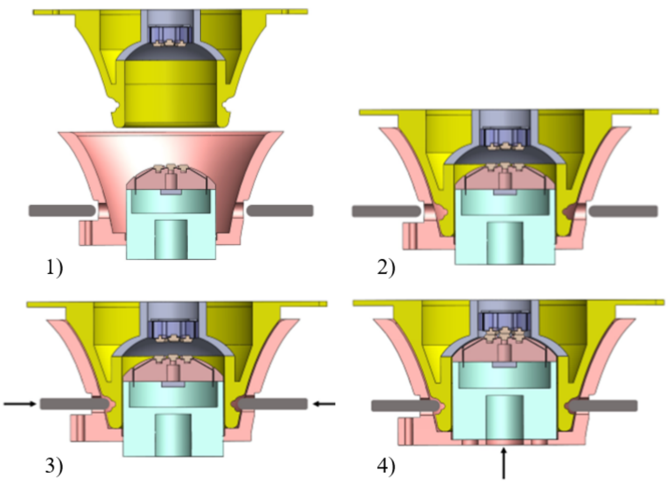

Figure 4: Docking sequence

DOI: 10.13009/EUCASS2017-169

In order to prevent the drone from yawing, a rubber strip is inserted inside the groove of the probe so that it can increase the grip between the radial pins and the probe. In case of failure of the locking mechanism, the peculiar geometry of the system ensures a good stability once the UAV lands in the correct position thanks to the central pin inside of the drogue.

2.3 Navigation system

The objective of the navigation subsystem is to determine the position and attitude of the UAV with respect to the docking station during the final approach and landing. This subsystem requires a higher accuracy than that needed for long distance GNC and so it must be designed specifically for the vertical cone volume above the docking station at a maximum height of about 2 m. In order to get the maximum flexibility, the subsystem should be able to operate in every scenario in which the flight of the UAV is permitted by the weather conditions (i.e. even during nighttime) and take up a minimal amount of space, weight and power on-board the UAV.
An architecture based on ultrasound sensors can provide a high accuracy on altitude determination on earth, but the weak propagation of ultrasonic waves on Mars atmosphere makes it unsuitable for such application.[20] Moreover, the determination of the horizontal position of the UAV over a quasi-flat ground is impossible with ultrasound sensors, unless a fixed ultrasonic emitter was placed on the docking station and ultrasound receivers on-board the multirotor.
A consolidated architecture in academic research for UAV navigation is based on Simultaneous Localization And Mapping (SLAM) and Laser Imaging Detection And Ranging (LIDAR) fusion.[4,9] Laser scanners offer a high accuracy on range determination and SLAM algorithms can reconstruct a 3D map of the surrounding environment. Such technique has been studied for indoor navigation as explained in the introduction, giving very promising results. However the application in a wide open, outdoor, GNSS-denied environment would not give the same accuracy because the landmark cloud would not be well defined and small displacements during the final approach of the UAV could be badly estimated by the algorithm.
In order to get a small and low-cost subsystem, we relied on computer vision using a small Raspberry Camera Module on-board the quadrotor and optical LED markers on the docking station as represented in Fig. (1). The camera has a maximum resolution of 3280×2464 pixels and a field of view of about 77 deg $\times$ 62 deg, is integrated on a Raspberry Pi 3 computation unit and uses the projection of the LEDs on the lens to determine the position and attitude of the FS with respect to the GS, as explained later in this section. Notice that the LED pattern is composed by five external blue markers and five internal red ones: the formers are used until they exit from the field of view of the camera (i.e. when the UAV is very close to the docking station) and the red ones are used for the very last centimeters of flight until docking is accomplished. The choice of using two LED patterns is due to the necessity of having a good sensor sensitivity at high distances and keeping always at least four LEDs in the field of view.
The navigation algorithm works in three phases for each image collected by the camera: it analyses the image to identify the LED projections on the image reference frame (*Image Analysis phase*), it associates each projection to the corresponding LED on the docking station (*Pattern Analysis phase*) and finally it estimates the position and attitude of the drone with respect to the LED pattern reference frame (*Pose Estimation phase*). Each phase is explained below:

1. *Image Analysis*: this is the most time-consuming phase and it is dynamically adjusted during the descent of the UAV in order to speed it up as much as possible. At the very beginning, the first image collected by the camera is fully analyzed to identify the features that could be the projections of the five LED markers according to color, shape and size tolerances. For all the following fames after the first, the image is cropped to limit the portion to analyze and the features are searched in bounded areas around the coordinates of the features in the previous image. Moreover, to speed up the *Image Analysis* algorithm, the resolution of the images collected is lowered during the descent of the UAV.
   In this first phase of the navigation algorithm, outliers may affect the correct identifications of the LEDs, thus a RANSAC may be implemented to improve the robustness. This has not been possible in the Autoport project due to the low performances of the Raspberry CPU but is feasible with a more powerful nVidia Jetson TX1 module. On the contrary, this unit is more expensive and does not provide standard ports to connect external devices (e.g. a camera).
   At the end of this first phase, the projections of the five LEDs of the pattern have been identified, but they have not been enumerated yet, so the algorithm does not know which feature is associated to the i^{th} LED.

2. *Pattern Analysis*: in this phase, each of the five features is associated to the corresponding LEDs using geometrical relations based on the algorithm proposed by Santos.[15] Thus, this phase provides the 2D coordinates $\vec{x}_i$ of the i^{th} LED, which has 3D coordinates $\vec{X}_i$ in the pattern reference frame. $\vec{X}_i$ and $\vec{x}_i$ are in homogeneous coordinates.

3. *Pose Estimation*: given the 2D coordinates $\vec{x}_i$ calculated previously and the known $\vec{X}_i$, the objective of this phase is to determine the position and attitude of the drone with respect to the LED pattern (i.e. the docking station).

DOI: 10.13009/EUCASS2017-169

We define three reference frames: D fixed with the drone, C with the camera (pointing outwards the lens) and P fixed with the LED pattern. The rotation matrix ${}^{C}_{P}\mathrm{R}$ from P to C and the translation vector ${}^{C}\vec{t}_{P}$ from P to C in the C reference frame relate the vectors $\vec{x}_i$ and $\vec{X}_i$ as described by the pin-hole camera model in Eq. (1).

$$\begin{bmatrix} \vec{x}_i \\ 1 \end{bmatrix} = \begin{bmatrix} f_x & 0 & c_x \\ 0 & f_y & c_y \\ 0 & 0 & 1 \end{bmatrix} \left[{}^{C}_{P}\mathrm{R} \,|\, {}^{C}\vec{t}_{P} \right] \begin{bmatrix} \vec{X}_i \\ 1 \end{bmatrix} \tag{1}$$

Note that the intrinsic matrix of the camera must be known. Eq. (1) can be written for each LED, thus we have a system of five vector-valued equations. This can be solved using the iterative Levenberg-Marquarth optimization algorithm that minimizes the re-projection errors.
Finally, the position and attitude of the drone with respect to the LED pattern (i.e. ${}^{P}\vec{t}_{D}$ and ${}^{P}_{D}\mathrm{R}$) can be calculated using equations (2).

$$\begin{aligned} {}^{P}_{D}\mathrm{R} &= {}^{C}_{P}\mathrm{R}^{-1} \cdot {}^{C}_{D}\mathrm{R} \\ {}^{P}\vec{t}_{D} &= {}^{C}_{P}\mathrm{R}^{-1}({}^{C}\vec{t}_{D} - {}^{C}\vec{t}_{P}) \end{aligned} \tag{2}$$

Vector ${}^{C}\vec{t}_{D}$ and matrix ${}^{C}_{D}\mathrm{R}$ are geometrical and known.

To improve the accuracy of the algorithm, each color pattern features one LED out of the plane with respect the others, resulting in an amplification of the sensibility of the pin-hole model to little pitch and roll movements.

3. Characterization of the subsystems, tests and results

3.1 Battery recharge system

The power connector introduced in section 2.1 needs to be accurately characterized in terms of contact resistance to properly design the recharge circuit.
The total contact area of the rivets is 13.25 mm^2, approximate constant for every yaw angle of landing of the UAV. The manufacturer states that a 2.75 N/mm^2 contact pressure is required to maintain low the contact resistance, this means that a force of at least 36.5 N must be induced between the poles. The vertical actuator of the docking mechanism ensures a 43 N force, so a good contact in the power connector is guaranteed. The actual electrical resistance on the connection interface has been measured and resulted on 15.25 mΩ for the positive pole and 2.45 mΩ for the negative one. So the recharge circuit has a total 17.70 mΩ resistance on the connector. Considering that the recharge current must be of the order of 5 A to recharge the battery in one hour, the nominal power dissipated by the power connector only is just 354 mW.
Concerning the wireless system, the proposed architecture is not axial-symmetric, so it is necessary to determine which is the maximum allowable yaw landing error. To do this, we measured the induced voltage on the receiver by the transmitter as function of the misalignment of the coils along three directions, as shown on the left hand side of Fig. (5). The resulting voltage is represented on the right hand side of Fig. (5), and we can see that the maximum allowable

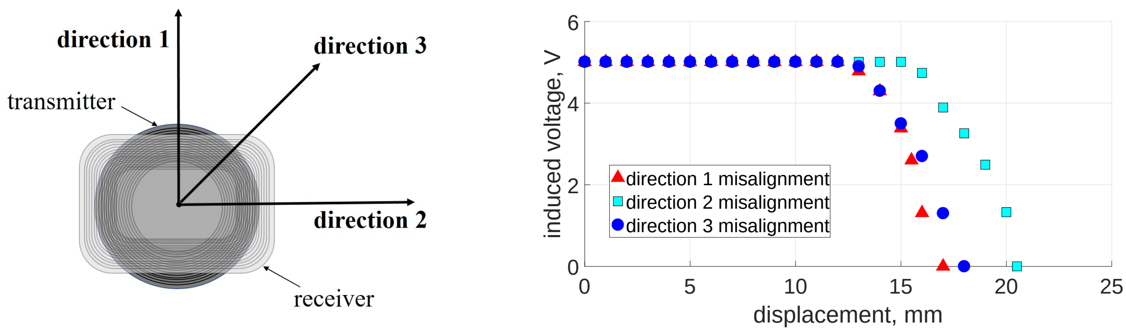

Figure 5: Induced voltage on the receiver coil as function of the misalignment

misalignment is of 12 mm. Supposing that the wireless receivers are installed under the arms of the quadrotor at a distance of 150 mm from the center of the docking mechanism, the maximum allowable yaw angle error is ±10 deg from the ideal yaw angle of docking. In the case that this tolerance is not respected, the battery will be recharged just with the power connector without balancing the cells

DOI: 10.13009/EUCASS2017-169

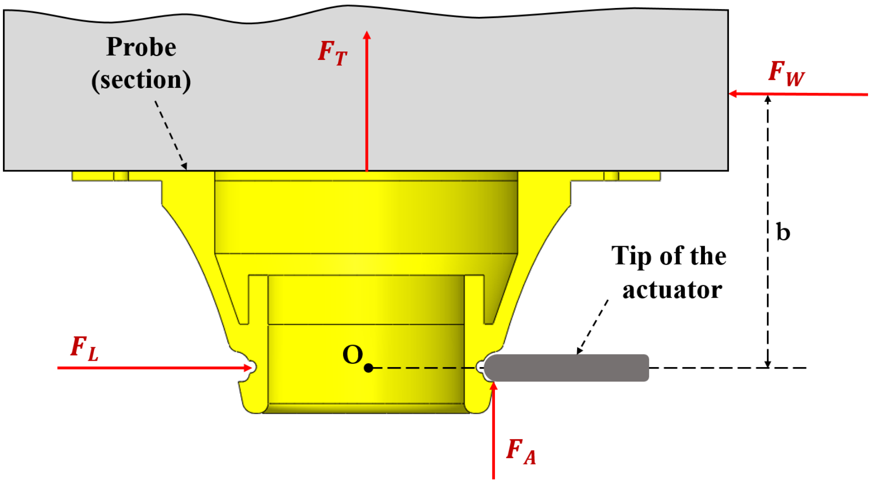

Figure 6: External forces applied on the docking mechanism

3.2 Docking mechanism

3.2.1 FEM simulations

To study the behavior of the Docking Mechanism under external loads, we made static FEM simulations. The three main external forces that may apply to the system are the locking force of the actuators F_L , the drag of the wind F_W and the thrust of the propellers F_T if the motors activate unexpectedly. These loads are represented in Fig. (6).

1. *Force of the actuators:* the locking force is assumed to be the one of the commercial actuators used, so F_L = 43 N. The related FEM simulation is represented in the first picture of Fig. (7): three forces were applied on the groove of the probe to simulate the activation of the three actuators. The maximum deformation produced is 0.003 mm and the maximum stress is 6.33 MPa. The ultimate strength, which is 50MPa, is reached with a force of 340 N which causes a deformation of 0.025 mm. The safety factor is 7.89.

2. *Drag of wind:* the wind force is given by $F_W = \frac{1}{2}\rho A c_D v^2$. In which ρ is the density of the atmosphere, A is the lateral area and it has been assumed to be that of the NASA Mars Scout concept of the UAV, so A = 0.2 m^2. v is the maximum velocity of the wind registered on the ground level of Mars, so v = 110 m/s. c_D is the drag coefficient and it has been assumed to be that of a cylinder with a medium Reynolds number, so c_D = 1.17. These values lead to a wind force F_W = 2 N. We decided to double the value of this force to simulate a disastrous scenario and we considered the force of the wind to be applied to the top of the probe as in Fig. (6). This simulation is reported in the second picture of Fig. (7). The maximum deformation produced is 0.002 mm and the maximum stress is 1.07 MPa. The ultimate strength is reached with a force of 210 N, which means a speed of wind of 877 m/s and a deformation of 0.1 mm. Such wind speed is unexpected on the surface of Mars.

3. *Thrust Force:* the thrust force is assumed to be the one of the propellers mounted on the commercial quadcopter used by Autoport, so F_T = 3.5 N. This simulation is represented in the third picture of Fig. (7). In this simulation, a force distribution is applied to the top of the probe. The maximum deformation and the maximum stress are respectively 0.0008 mm and 0.08 MPa. The ultimate strength is F = 2300 N which generates a deformation of 0.5 mm.

4. *Actuator Force:* the wind force may apply to the UAV and generate a momentum about the point O on the mechanism. This momentum loads the tip of the actuator with a vertical force F_A at the distance b with respect to the center O, as in Fig. (6). With the above F_W, the force F_A results to be 3 N. This simulation is represented in the fourth picture of Fig. (7).
   This force causes a deformation of 0.016 mm and a maximum stress of 7.7 MPa on the tip of the actuator. The estimated yield is about 100 N which causes a deformation of 0.196 mm. In the worst case possible, the force F_A would also be summed up along with the forces of pre-loading and vertical traction, however the above yield load would not be reached in any case.

DOI: 10.13009/EUCASS2017-169

5. *Thermal load:* the last FEM analysis was performed on the thermal expansion caused by the large thermal excursion present on Mars that goes from a minimum temperature of -140 °C to a maximum temperature of 20 °C. The result shows a deformation of 0.04 mm, which does not affect the behaviour of the mechanism. This simulation is represented in the fifth picture of Fig. (7).

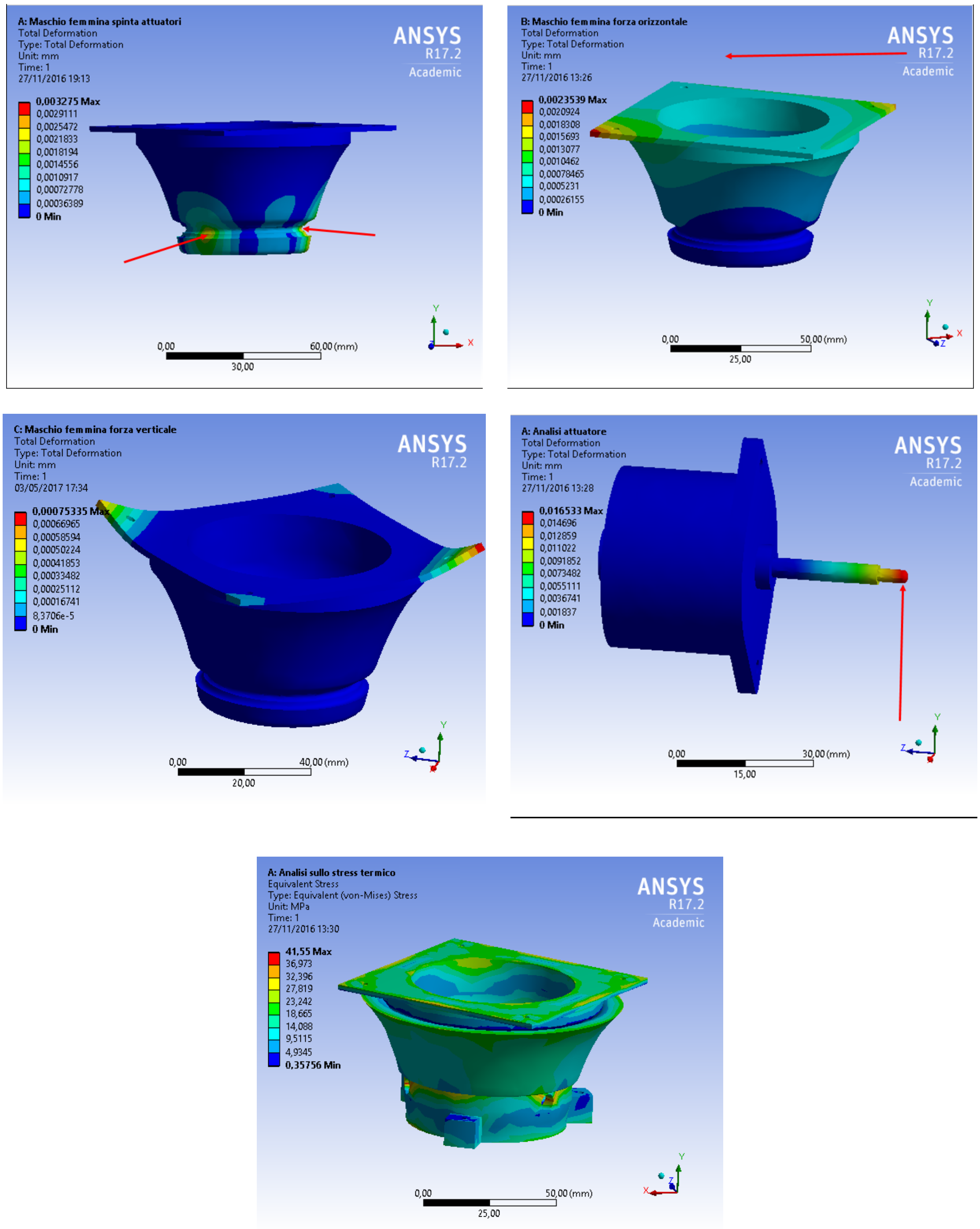

Figure 7: FEM simulations

The results of the FEM simulations are summarized in tables 1 and 2 . In particular the table 1 lists the results of the simulations in terms of maximum stress and maximum deformation induced by the forces above. On the contrary, table 2 takes in input the ultimate strength of the materials used for the mechanism and lists the values that the above forces must reach to break it. These tables demonstrate the strength of the mechanism and validate the possibility of use this design also in high-load scenarios.

DOI: 10.13009/EUCASS2017-169

Table 1: Results of the simulations on the load inducted by the external forces

Force	Value	Maximum deformation	Maximum stress
Locking force on the probe, F_L	43 N	0.003 mm	6.33 MPa
Wind force on the probe, F_W	4.5 N	0.02 mm	1.07 MPa
Thrust force on the probe, F_T	3.5 N	0.0008 mm	0.08 MPa
Vertical force on the actuators, F_A	3 N	0.016 mm	7.7 MPa

Table 2: Results of the simulations on the maximum allowable forces

Ultimate strength[2,8]	Force investigated	Maximum allowable force	Maximum deformation	FoS
50 MPa	F_L	340 N	0.025 mm	7.89
50 MPa	F_W	210 N	0.1 mm	46.7
50 MPa	F_T	2300 N	0.5 mm	625
250 MPa	F_A	100 N	0.196 mm	32.46

3.2.2 Horizontal and angular misalignment

Thanks to its the particular shape, the probe slides inside the drogue even without a perfect alignment. Numerous tests have been performed to measure the maximum misalignment tolerated by the mechanism: Fig. (8) represents the testbed used and the relative results. As we can see, the probe does not enter the drogue at some positions, resulting in a failed docking. This issue is caused by the central pin, which may obstruct the entrance of the probe. To fix this problem, the central pin will be shorten and more test are scheduled.

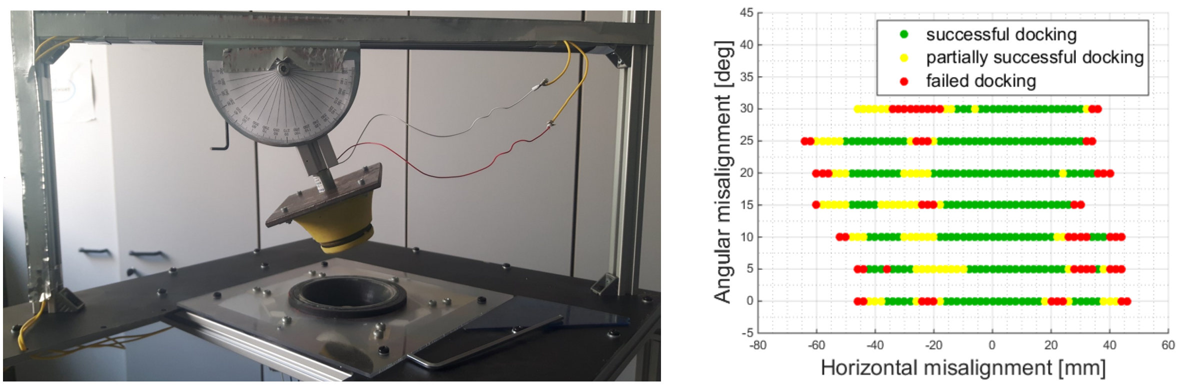

Figure 8: Misalignment test on docking mechanism

3.3 Navigation system

To test the navigation subsystem, we performed both static and dynamic measurements using the testbed in Fig. (9). We mounted the LED pattern on a three degrees of freedom (two translational, one rotational) platform moved by a computer, while the camera was placed on a fixed structure. On the left hand side of Fig. (9), the reference system T is world fixed, while P if fixed to the LED pattern and can translate along y_T and z_T, and rotate along x_P. In this configuration the camera is mounted in C and the LED pattern is moving, but we will comment our results as if the P reference frame is fixed and the camera reference frame C is moving, as represented in the right hand side of Fig. (9). The testbed permits a maximum displacement of ±200 mm along y_T, 0-835 mm along x_T and a maximum rotation of ±180 deg around x_P. To estimate the position and attitude of the camera with respect to the LED pattern, we used the blue LEDs when ${}^{P}z_C$ ≥400 mm and the red LEDs for ${}^{P}z_C$ <400 mm.

DOI: 10.13009/EUCASS2017-169

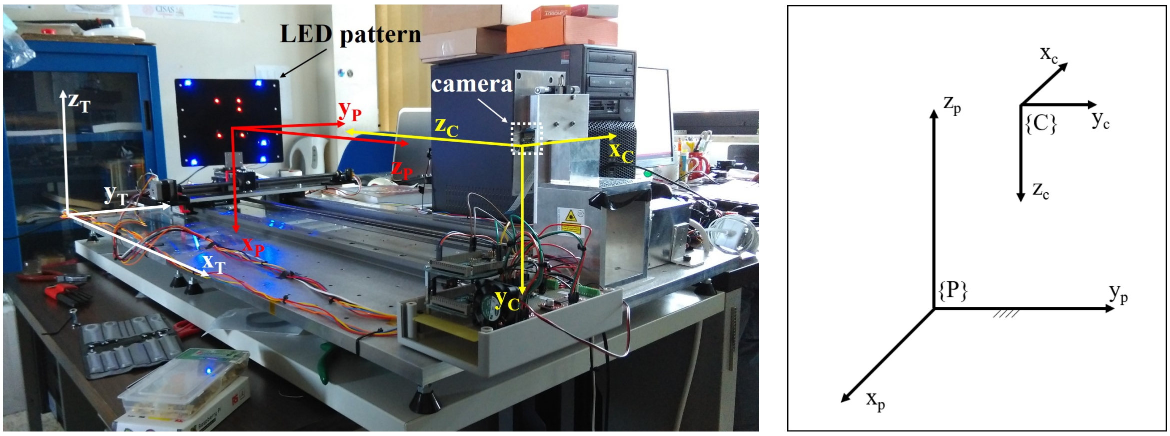

Figure 9: The testbed and the reference frame for the navigation tests

3.3.1 Static tests

The static tests have been performed on 140 photos taken with the camera at different positions and angles of the LED pattern. A Monte Carlo method has been applied several times to each photo, and each time the navigation algorithm has estimated the position and attitude of C with respect to P. In the Monte Carlo, the random white noises listed in table 3 have been added to the vectors $\vec{x}_i$ and $\vec{X}_i$ in order to evaluate the accuracy and precision on the estimation of ${}^P_C\mathrm{R}$ and ${}^P\vec{t}_C$.

Table 3: Random noises considered using the Method of Monte Carlo

Vector	White noise	Source
$\vec{x}_i$	±0.22 pixels	Error in the determination of the position of the centroid of the LEDs in the image frame
$\vec{X}_i$	±0.2 mm	Mechanical defect in the mounting holes of the LEDs in the pattern

Table 4: Static tests results

	Blue LED pattern		Red LED pattern	
Coordinate	Accuracy	Precision (1 sigma)	Accuracy	Precision (1 sigma)
X	4.20 mm	4.37 mm	3.79 mm	4.31 mm
Y	8.08 mm	4.99 mm	4.57 mm	6.42 mm
Z	3.97 mm	1.65 mm	4.39 mm	2.72 mm
Roll	0.89 deg	0.42 deg	0.91 deg	1.42 deg
Pitch	0.34 deg	0.34 deg	0.71 deg	0.84 deg
Yaw	0.12 deg	0.07 deg	0.18 deg	0.19 deg

The mean results of the static tests are reported in table 4. It should be noted that, even with artificial random noises, the performances of the algorithm are very good: the uncertainty on the position and attitude is much lower than the maximum misalignment tolerated by the docking mechanism as reported in section 3.2.

3.3.2 Dynamic tests

To test the algorithm in dynamic conditions, the LED pattern has been moved continuously along x_T and y_T, without rotating around the x_P axis, with a 1.5 Hz tracking rate of the camera. This is the maximum frequency achievable by the Raspberry Camera Module and the Raspberry Pi 3 unit, making these COTS unsuitable to control the UAV.
Three different trajectories have been tested and the second one is represented in Fig. (10) and Fig. (11). Note that the algorithm can track the real trajectory with very good accuracy, but some frames may be skipped by the Raspberry due to the poor quality of the CPU. Despite of this issue, the overall mean errors evaluated during the three dynamic tests, listed in table 5, are very satisfactory. Further analysis are needed to assess the performances of the algorithm at higher

DOI: 10.13009/EUCASS2017-169

distances of the camera with respect to the LED pattern. Moreover, a faster CPU, such as a nVidia TX1 module, is necessary to estimate the position and attitude of the UAV at a sufficiently high frequency for control purpose.

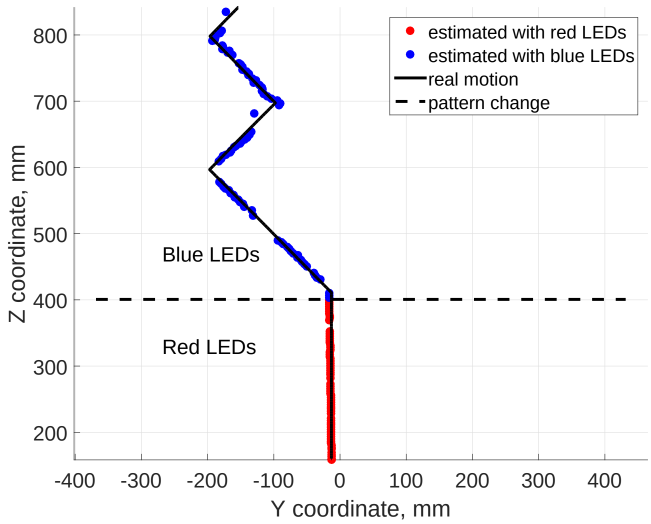

Figure 10: Trajectory of the camera during the second dynamic test

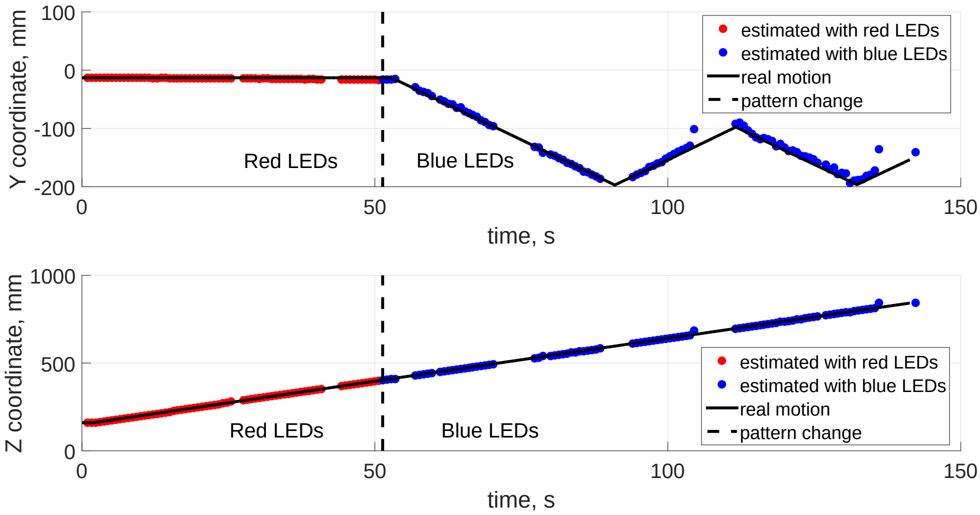

Figure 11: Y and Z coordinates of the camera as function of time during the second dynamic test

Table 5: Overall errors of the pose estimation in the dynamic tests

	First test		**Second test**		**Third test**	
Coordinate	**Red pattern**	**Blue pattern**	**Red pattern**	**Blue pattern**	**Red pattern**	**Blue pattern**
X	1.67 mm	5.43 mm	2.01 mm	5.06 mm	2.12 mm	4.37 mm
Y	1.01 mm	2.50 mm	1.34 mm	4.28 mm	1.06 mm	1.98 mm
Z	2.89 mm	3.01 mm	2.73 mm	2.23 mm	4.34 mm	6.81 mm
Roll	0.24 deg	0.56 deg	0.21 deg	0.90 deg	0.12 deg	0.82 deg
Pitch	0.09 deg	0.16 deg	0.03 deg	0.21 deg	0.88 deg	0.11 deg
Yaw	0.01 deg	0.03 deg	0.01 deg	0.10 deg	0.03 deg	0.05 deg

DOI: 10.13009/EUCASS2017-169

4. Conclusion

In this paper we presented the architecture proposed by the Autoport Project to develop a suite of sensors and mechanism for planetary UAVs, capable of landing, docking and recharging the battery of a small quadrotor. We used COTS as much as possible in every subsystem, but some custom components had to be developed to meet the requirements and keep the overall cost of the system low. Table 6 resumes the components chosen and those discharged.

Table 6: Components selected and discharged

Subsystem	**Component**	**Type**	**Used**	**Note**
Recharge	Qi wireless coils	COTS	yes	low-weight and highly efficient component
	power connector	custom	yes	necessity of a high power component housed inside of the docking mechanism
	NFC	COTS	no	no high power COTS available
	SkySense charging pad	COTS	no	expensive solution
Docking	linear actuator	COTS	yes	low-cost and reliable COTS available
	probe and drogue	custom	yes	no COTS available
Navigation	Raspberry Pi 3	COTS	yes	open-source board with an integrated camera module
	Raspberry camera module	COTS	yes	high resolution component integrated on the Raspberry Pi 3 board
	visible LEDs	COTS	yes	stable environmental noise on visible spectrum
	infra-red LEDs	COTS	no	higher environmental noise on IR spectrum
	Raspberry Pi NoIR camera	COTS	no	higher environmental noise on IR spectrum

The battery recharge system has been designed integrating COTS and custom components, with both wireless and contact parts cooperating to recharge the LiPo battery, balance the cells and so maximize the operational life. The system has not been fully tested yet, but the architecture proposed is promising for fast recharge without compromising the health of the battery.
The docking mechanism has been demonstrated to be strong and lightweight and thanks to its scalable shape sets a new design for many spacecraft applications. Moreover, the lack of complex parts makes it suitable for human-denied environments and for low-power vehicles such as educational cubesats.
The navigation platform developed takes advantage of computer vision algorithms to determine the position and attitude of the UAV with enough accuracy. However, the limited speed of the hardware makes it unsuitable for control purpose. As explained in section 2.3, a better performing CPU is necessary to use the algorithm in a real landing scenario.

5. Acknowledgments

The authors wish to thank all the students that worked on the Autoport Project: Francesco Andreace, Nicola Bagarello, Nicolò Borin, Marina Cañete Muñoz, Alberto Cenzato, Alessandro Colovini, Giulio de Pieri, Dario Franchin, Stefano Gragnaniello, Christian Isone, Francesco Longhi, Matteo Meneghel, Gabriele Palano, Giulio Peloso, Alessandro Reffo, Alessandro Rossi, Daniele Scelsa, Riccardo Tonello and Mirko Zigliotto.
Morehover, a special thanks goes to Professor Angelo Cenedese and his fellow researchers Gianluca Giorgini and Davide Bosello for the precious advices and their support during the tests made in their laboratory at the Department of Information Engineering.
Last, the authors thank the University of Padua for the financial support in the development of the project.

References

[1] M. Barbetta, A. Boesso, F. Branz, A. Carron, L. Olivieri, J. Prendin, F. Rodeghiero, L. Savioli, F. Spinello, and A. Francesconi. ARCADE-R2 Experiment On Board BEXUS 17 Stratospheric Balloon. *CEAS Space Journal*, 7(3):347–358, September 2015.

[2] H. Bowes, T. Russell, and T. Suter. *Mechanics of Engineering Materials*. John Wiley and Sons, 1984.

DOI: 10.13009/EUCASS2017-169

[3] A. Compagnin, A. Cenzato, E. Lungavia, N. Bagarello, A. Rossi, A. Reffo, R. Mantellato, L. Olivieri, F. Sansone, and A. Francesconi. Autoport Project: a Docking Station for Planetary Exploration Drones. Grapevine, TX, USA, January 2017. AIAA. SciTech forum.

[4] S. Grzonka, G. Grisetti, and W. Burgard. Towards a Navigation System for Autonomous Indoor Flying. Kobe, Japan, May 2009. IEEE. International Conference on Robotics and Automation.

[5] J.F. Gundlach. Unmanned Solar-Powered Hybrid Airships for Mars Exploration. Reno, NV, USA, January 1999. AIAA. Aerospace Sciences Meeting and Exhibit.

[6] A.B. Junaid, Y. Lee, and Y. Kim. Design and Implementation of Autonomous Wireless Charging Station for Rotary-Wing UAVs. *Aerospace Science and Technology*, 54:253–266, July 2016.

[7] F.P. Kemper, K.A.O. Suzuki, and J.R. Morrison. UAV Consumable Replenishment: Design Concepts for Automated Service Stations. *Journal of Intelligent and Robotic Systems*, 61(1):369–397, January 2011.

[8] S.M. Lee. *International encyclopedia of composites*, volume 1. VCH Publishers, 1990.

[9] R. Li, J. Liu, L. Zhang, and Y. Hang. LIDAR/MEMS IMU Integrated Navigation (SLAM) Method for a Small UAV in Indoor Environments. Karlsruhe, Germany, September 2014. IEEE. Inertial Sensors and Systems Symposium.

[10] D. Miller, A. Saenz-Otero, J. Wertz, A. Chen, G. Berkowski, C. Brodel, S. Carlson, D. Carpenter, S. Chen, S. Cheng, D. Feller, S. Jackson, B. Pitts, F. Perez, J. Szuminski, and S. Sell. SPHERES: a Testbed for Long Duration Satellite Formation Flying in Micro-Gravity Conditions. *Advances in the Astronautical Sciences*, 105, January 2000.

[11] Y. Mulgaonkar. Automated Recharging for Persistence Missions with Multiple Micro Aerial Vehicles. Master's thesis, University of Pennsylvania, 2012.

[12] L. Olivieri and A. Francesconi. Design and Test of a Semiandrogynous Docking Mechanism for smallsatellites. *Acta Astronautica*, 122:219–230, February 2016.

[13] J.C. Pavlich, P.Jr. Tchoryk, A.B. Hays, and G. Wassick. KC-135 Zero-G Testing of a Microsatellite Docking Mechanism. *Space Systems Technology and Operations*, 5088, August 2003.

[14] F. Sansone, A. Francesconi, L. Olivieri, and F. Branz. Low-Cost Relative Navigation Sensors for Miniature Spacecraft and Drones. Benevento, Italy, August 2015. IEEE. Metrology for Aerospace.

[15] P. Santos, A. Stork, A. Buaes, and J. Jorge. Innovative Geometric Pose Reconstruction for Marker-based Single Camera Tracking. Hong Kong, China, 2006. ACM. International Conference on Virtual reality Continuum And Its Applications.

[16] M.C. Silverman, B. Jung, D. Nies, and S G. Sukhatme. Staying Alive Longer: Autonomous Robot Recharging put to the Test. Technical report, 2003.

[17] K.A. Swieringa, C.B. Hanson, J.R. Richardson, J.D. White, Z. Hasan, E. Qian, and A. Girard. Autonomous Battery Swapping System for Small-Scale Helicopters. Anchorage, AK, USA, May 2010. IEEE. International Conference on Robotics and Automation.

[18] G. Tournier, M. Valenti, J. How, and E. Feron. Estimation and Control of a Quadrotor Vehicle Using Monocular Vision and Moiré Patterns. Keystone, CO, USA, August 2006. AIAA. Guidance, Navigation, and Control Conference and Exhibit.

[19] K.E. Wenzel, A. Masselli, and A. Zell. Automatic Take Off, Tracking and Landing of a Miniature UAV on a Moving Carrier Vehicle. *Journal of Intelligent and Robotic Systems*, 61(1):221–238, March 2011.

[20] J Williams. Acoustic Environment of the Martian Surface. *Journal of Geophysical Research*, 106(E3):5033–5041, March 2001.

[21] L.A. Young. Vertical Lift: Not Just For Terrestrial Flight. Arlington, VA, USA, October 2000. AIAA. International Powered Lift Conference.

DOI: 10.13009/EUCASS2017-169

[22] L.A. Young, R.T.N Chen, E.W. Aiken, and G.A. Briggs. Design Opportunities and Challenges in the Developement of vertical Lift Planetary Aerial Vehicles. San Francisco, CA, USA, 2000. American Helicopter Society. International Vertical Lift Aircraft Design Specialist's Meeting.

[23] L.A. Young, V. Gulick, E.W. Aiken, R. Mancinelli, and G.A. Briggs. Rotorcraft as Mars Scouts. Big Sky, MT, USA, March 2000. IEEE. Aerospace Conference.